Rare Met. (2019) 38(5):413–419
https://doi.org/10.1007/s12598-019-01259-6

RARE METALS
www.editorialmanager.com/rmet

Bifunctional metal–organic frameworks toward photocatalytic CO_2 reduction by post-synthetic ligand exchange

Xiao-Hui Chen, Qin Wei, Jin-Dui Hong, Rong Xu, Tian-Hua Zhou*

Received: 3 January 2019 / Revised: 21 February 2019 / Accepted: 18 March 2019 / Published online: 16 April 2019

Abstract Photocatalytic reduction of CO_2 to useful fuel has been identified as a promising strategy to address the energy and environmental issues. Development of well-defined photocatalysts toward CO_2 reduction has attracted increasing interest to gain insight into the reactive mechanism. Herein, by post-synthetic ligand exchange, a bifunctional Re-based metal–organic framework (MOF) was successfully prepared. It not only serves as a photosensitizer but also acts as a catalyst for photochemical reduction of CO_2. Furthermore, it is found that a Re-based MOF containing 30% Re-based ligands displays improved activity compared to MOF with 100% Re-based ligands. This work provides clues to the design and synthesis of bifunctional MOFs toward photocatalytic CO_2 reduction.

Keywords Photocatalysis; Metal–organic framework (MOF); CO_2 reduction; Post-synthesis

1 Introduction

With the development of human activities, the excessive emission of carbon dioxide (CO_2) results in an increasingly serious environmental problem. Artificial photosynthesis using abundant natural resources such as H_2O and CO_2 to produce hydrogen and value-added fuels has been considered as the most promising solution to address this issue [1–10]. One of the most promising processes is the direct photochemical reduction of CO_2 into chemicals or fuels such as methane, methanol, carbon monoxide, and formic acid [11–14]. Among these products, the two-electron reduction of CO_2 to CO is of great significance for the chemical industry. To date, considerable effort has been devoted to develop the catalysts for selective reduction of CO_2 to CO [15–17]. It has been demonstrated that precious metals such as Ag, Au, and its alloys are the most active co-catalysts for CO_2 reduction to CO [18–20]. Development of well-defined catalysts with high efficiency and selectivity still remains great challenges.

Metal–organic frameworks (MOFs) are widely employed as promising materials for gas storage, magnetism, luminescence, adsorption, and heterogeneous catalysis [21–27]. Owing to their controllable chemical and physical properties, MOFs are also attractive candidates toward photocatalytic solar fuel production [22]. A few MOFs have been employed as photocatalytic hydrogen evolution materials [28, 29]. To construct this type of functional materials, two common strategies have been developed so far. One approach is the introduction of visible-light absorbing organic ligands into the framework such as porphyrin [30–35]. Another method is doping MOF with visible-light absorbing metal complex. For example, Lin's group [36, 37] has reported a photocatalytically active MOF by doping the Ir-based complex into the UiO-67 framework. However, in these reported systems, Pt nanoparticles are often used as co-catalysts [30, 37]. In our group, we developed a new strategy to synthesize a

X.-H. Chen, Q. Wei
School of Chemical Engineering, Fuzhou University, Fuzhou 350002, China

J.-D. Hong, R. Xu
School of Chemical and Biomedical Engineering, Nanyang Technological University, Singapore 637459, Singapore

T.-H. Zhou*
State Key Laboratory of Structural Chemistry, Fujian Institute of Research on the Structure of Matter, Chinese Academy of Sciences, Fuzhou 350002, China
e-mail: Thzhou@fjirsm.ac.cn

bifunctional photocatalytically active MOF (MOF-253-Pt), which serves as not only a photosensitizer but also a photocatalytic site by inserting platinum species into MOF-253 that has an accessible 2,2′-bipyridine unit on the framework [38]. By the coordination of Pt ions to bipyridine unit, the MOF possesses extra ultraviolet–visible (UV–Vis) absorbing edge centered at 410 nm with additional extended absorption edge of 650 nm. This result indicates that MOF-253-Pt can serve as a photosensitizer. Under the optimization condition, the MOF-253-Pt displays the amount of hydrogen evolution almost five times greater than the corresponding metal complex.

However, only a few MOFs and MOF-derived nanomaterials were reported for photocatalytic CO_2 reduction [33, 35, 39–43]. One of the bottlenecks is the limitation in introducing active metal sites capable of photocatalytic CO_2 reduction into the MOF framework. Recently, Li's group [44] reported the introduction of Ti into UiO-66, which displays more efficient CO_2 reduction compared to TiO_2 due to the improved electron transfer into the MOF. Consequently, by doping Re complex into MOFs, many groups also reported such MOFs capable of CO_2 reduction [36]. One of the drawbacks of the strategies mentioned above is to synthesize the functional MOF through solvothermal method, which restricts the introduction of thermally unstable metal complexes.

In this work, we report a new approach to construct Re-based MOF by post-synthetic ligand exchange (PSLE) at room temperature (Fig. 1). This strategy can be employed to introduce some active metal complexes into MOF which are instable under hydro- or solvothermal conditions [45, 46]. Furthermore, the strategy allows us to systematically study the reaction mechanism through tuning the amount of the introduced metal complexes by means of controlling the reaction time.

2 Experimental

2.1 Materials and methods

2,2′-bipyridine-5,5′-dicarboxylic acid, 4,4′-biphenyldicarboxylic acid, and pentacarbonylchlororhenium(I) were obtained from Sigma-Aldrich and used as received. $ZrCl_4$, benzoic acid, and triethanolamine (TEOA) were obtained from Alfa Aesar. CH_3CN was purchased from Kanto Chem. Co., Inc. All other chemicals were obtained from Merck and used without further purification. Fourier transform infrared spectroscopy (FTIR) spectra were collected with a PerkinElmer FTIR Spectrum GX in the range of 4000–400 cm^{-1}. Elemental analysis (C, H, N) was performed on an Elementary Vario El III instrument. Powder X-ray diffraction (XRD) patterns were obtained on a Bruker AXS D2 Advanced X-ray diffractometer with monochromatized Cu Kα radiation (λ = 0.154056 nm, 40 kV and 20 mA). The data were collected in a range of 5°–65° and a step size of 0.01 (°)·s^{-1}. All measurements were performed at room temperature and atmospheric pressure. UV–Vis diffuse reflectance spectra (UV–Vis DRS) were obtained by UV–Vis absorption spectroscopy (UV-2450, Shimadzu). Brunauer–Emmett–Teller (BET) surface area was measured by N_2 adsorption and desorption at 77 K using a Micromeritics ASAP 2020 apparatus and a Quantachrome Autosorb-6 sorption system. Samples were degassed over offline system at 150 °C for 12 h under vacuum before analysis. Field emission scanning electron microscopy (FESEM) specimen was prepared through dropping the samples on a silicon substrate followed by air-drying at room temperature. The measurements were performed on a JSM-6700F (JEOL) microscopy.

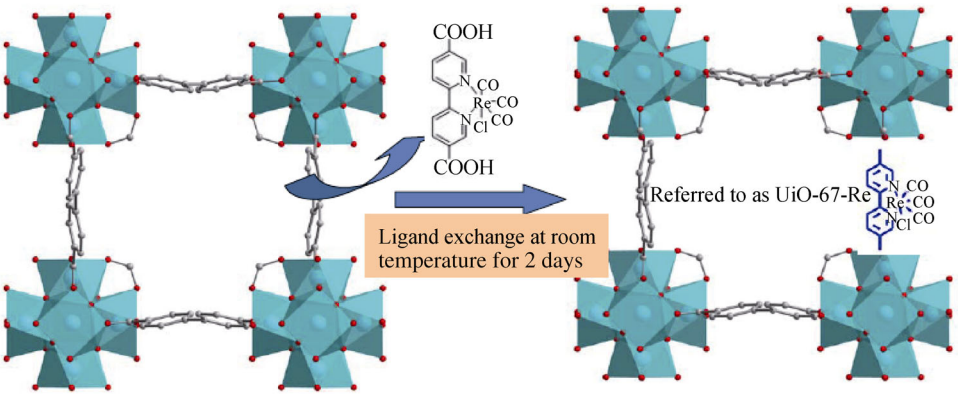

Fig. 1 Schematic representation of post-synthetic exchange (PSE) of UiO-67-Re MOF

2.2 Preparation of UiO-67

UiO-67 was prepared according to the reported procedure with slight modifications [47]. $ZrCl_4$ (24 mg), 4,4′-biphenyldicarboxylic acid (25 mg), and benzoic acid (67 mg) were dissolved in 5 ml N,N′-dimethylformamide (DMF). After ultrasonication for 30 min, the mixture was heated to 120 °C in an oven in a 20 ml glass vial. After 24 h, the vial was cooled to room temperature. The precipitates were obtained by centrifugation. Then, the powders were suspended in DMF (10 ml). After stirring at room temperature for 2 h, the suspension was isolated by centrifugation and the obtained powders were re-dispersed in 10 ml ethanol. After standing at room temperature for 12 h, the powders were obtained by centrifugation and dried under vacuum at 150 °C.

2.3 Post-synthetic exchange between UiO-67 and Re complex

Tris-carbonyl-chloro(5,5′-dicarboxyl-2,2′-bipyridine)rhenium(I) (referred to as Re complex) was synthesized according the previously described method [36]. Re complex (100 mg, 0.2 mmol) was dissolved in aqueous 4% KOH solution (4 ml) at room temperature. After stirring for 6 h, the mixture was neutralized to pH 7 with 1 mol·L^{-1} HCl, and then UiO-67 (71 mg, 0.2 mmol) was added to the solution. The mixture was left standing for 5 days, and the precipitates were isolated by centrifugation and washing with methanol three times. The final solids were re-dispersed in 10 ml methanol. After 24 h, the solid was centrifuged and the methanol was decanted. The fresh methanol (10 ml) was re-added to the solids. This methanol soaking procedure was repeated three times (24 h each). Finally, after centrifugation, the powders were dried under vacuum overnight at 50 °C. Then, the powders were suspended in 10 ml methanol-d_4 at room temperature for 1, 2, or 5 days. The mixture was centrifugated and the methanol-d_4 was collected and used for ^{1}H nuclear magnetic resonance (NMR) analysis. Finally, the powders obtained (referred to as UiO-67-Re-30%) were dried under vacuum overnight at 50 °C. The solids (9.4 mg) were digested with 40 μl 48% HF which was diluted with 580 μl DMSO-d_6 and used for ^{1}H NMR.

2.4 Preparation of UiO-67-Re-100%

Re complex (171.5 mg, 0.343 mmol) and $ZrCl_4$ (84 mg, 0.343 mmol) were dissolved in 20-ml DMF in a Teflon-lined stainless steel autoclave (23 ml). Then, 0.7 ml acetic acid was added. The mixture was stirred for 30 min and then heated to 120 °C for 24 h. After cooling to room temperature, the yellow precipitates were collected by centrifugation and washed with ethanol three times. The final yellow powders were dried under vacuum at 150 °C overnight and used as photocatalyst for CO_2 reduction.

2.5 Photocatalytic CO_2 reduction measurement

Visible-light-driven CO_2 reduction reaction was performed in a closed gas circulation and evacuation system with a Pyrex cell. The photocatalysts were added to a 50-ml mixture consisting of triethanolamine (TEOA), H_2O, and CH_3CN under vigorous stirring. The pH value of the TEOA solution was adjusted to 8.5 by adding concentrated HNO_3 solution (69 wt%). A 300-W Xenon lamp was employed as the light source with cut-off filter (> 420 nm). The reaction temperature remained around 20 °C with a cooling water jacket. Before reaction, the mixed solution was saturated with CO_2 at 100 kPa. The photocatalytic product was detected using an online gas chromatography (Agilent 7820B).

2.6 Calculation of number of moles of MOF catalyst (UiO-67-Re-30%)

Based on the molecular formula and 30% (0.30769) replacement of 4,4′-biphenyldicarboxylic acid (BPDC) linkers by catalyst, the molecular formula is defined as $Zr_6O_4(OH)_4\cdot[0.6(C_{14}H_8O_4)\cdot0.4(C_{15}H_6ClN_2O_7Re)]_6\cdot10H_2O$. And the mass of elements was calculated as: C, 34.14; H, 2.23; Cl, 2.80; N, 2.21; O, 25.90; Re, 14.70; Zr, 18.01.

3 Results and discussion

The UiO-67 framework ($Zr_6O_4(OH)_4(BPDC)_6$), consisting of Zr(IV)-based secondary building units (SBUs) and the 4,4′-biphenyl dicarboxylic acid (BPDC) ligand, was chosen as the prototype for preparation of the functional MOF because it displayed high structural stability with respect to water. The crystalline UiO-67 was synthesized using $ZrCl_4$, BPDC, and benzoic acid in DMF for 24 h under solvothermal conditions. After cooling to room temperature, the crystals were washed with MeOH (methanol) and then activated under vacuum. FESEM indicated an octahedral morphology of the UiO-67 crystals obtained with a particle size ranging from 50 to 100 nm (Fig. 2a). For comparison, the Re complex [$Re(CO)_3(dcpy)Cl$] (H_2L_4) was also synthesized by refluxing the mixture of (2,2′-bipyridine)-5,5′-dicarboxylic acid (DCPY) and pentacarbonylchlororhenium(I) according to the method in Ref. [36]. The H_2L_4 was characterized by NMR spectroscopy. Then, the reaction between the metal complex H_2L_4 and $ZrCl_4$ in DMF produces UiO-67-Re-100% (referred to as UiO-67-Re). Taking the advantage of the structural

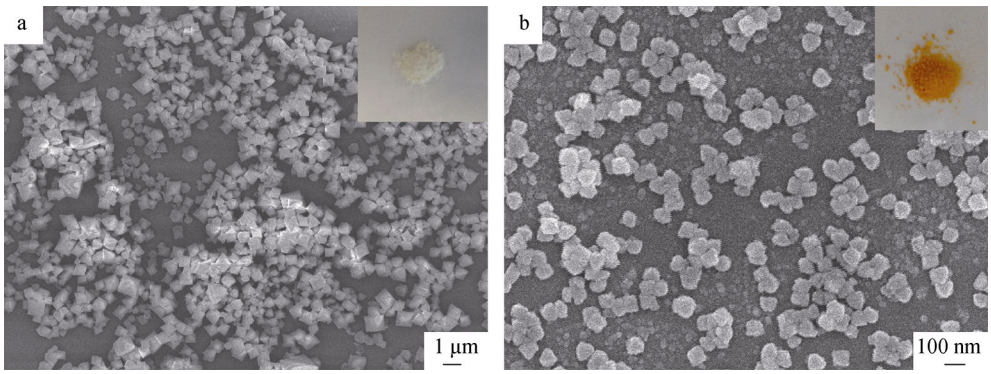

Fig. 2 FESEM images of **a** UiO-67 and **b** UiO-67-Re-30%

homology of the BPDC ligand in UiO-67 and dcpy ligand in Re complex, theoretically we could employ PSLE to access a series of Re-based MOF with different contents of Re complexes (Fig. 1). According to the literature method [48], the use of ultrapure water produced a series of UiO-67-Re at room temperature with the reaction time changing from 24 to 120 h. In this work, the ligand-exchanged MOF, UiO-67-Re-30%, was isolated as an orange microcrystalline powder after exchanging for 2 days. The resultant powders were washed thoroughly with fresh MeOH and activated under vacuum. As a result, the activated UiO-67-Re-30% displays a BET surface area of 490 $m^2 \cdot g^{-1}$ (Fig. 3a). The value is lower than that of other MOF UiO-67 (1015 $m^2 \cdot g^{-1}$), suggesting that PSLE process indeed has occurred between UiO-67 and Re complex, implying that the Re complex was not simply inserted in the MOF pores. Thus, the PSLE process would result in a much lower surface area. FESEM images show that the UiO-67-Re-30% preserves the morphological features of UiO-67 with slight variation in size, indicative of a solid-state PSLE mechanism (Fig. 2b). However, powder XRD patterns before and after PSLE confirm that the framework of UiO-67 remains unchanged (Fig. 3b).

To confirm the degree of PSLE, proton magnetic resonance spectroscopy (^{1}H NMR) was characterized. Treatment of UiO-67-Re-30% with dilute HF/d_6-DMSO was used to digest the MOF and decompose Re-complex to DCPY. The ^{1}H NMR confirmed the degree of PSLE is 30%, giving an overall formula of $Zr_6O_4(OH)_4(bpdc)_{4.2}(Re(CO)_3(dcpy)Cl)_{1.8} \cdot 2CH_3OH$ (Fig. 4a). To further confirm that Re complex was incorporated into the framework instead of trapping in the pores of the MOF, additional experiments were carried out. The UiO-67-Re-30% was soaked in the d_4-CH_3OH. As shown in Fig. 4b, the absence of ^{1}H NMR of the dcpy was observed in the supernatant. The observations are also indicative of a ligand exchange process and exclude the presence of Re complex trapped in the pores of the MOF. Based on the observation above, these results provide consistent evidences with the reported PSLE studies. This observation indicates the Re complex anchors on the UiO-67 framework through a ligand PSLE process.

To further demonstrate the successful incorporation of the Re complex into MOF, FTIR and UV–Vis DRS were employed. FTIR spectrum of UiO-67-Re exhibits two obvious CO-stretching vibration bands at 2033 and 1905 cm^{-1}. By contrast, such absorption bands were not observed for the UiO-67 between 2100 and 1900 cm^{-1} (Fig. 5a). Furthermore,

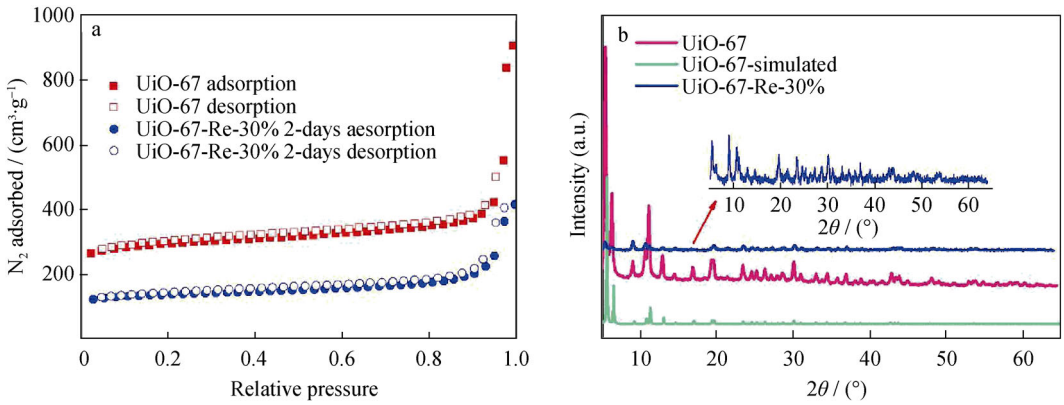

Fig. 3 **a** N_2 absorption/desorption isotherms of UiO-67 and UiO-67-Re-30% and **b** XRD patterns of UiO-67 and UiO-67-Re-30%

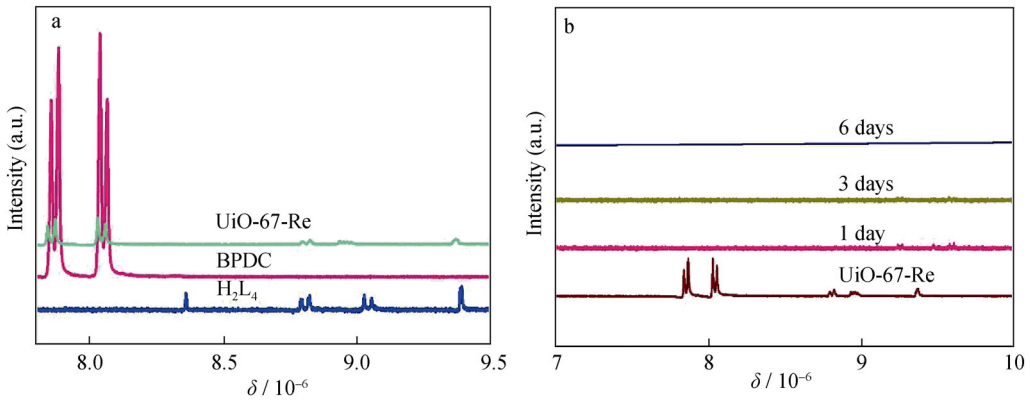

Fig. 4 ^{1}H NMR spectra of **a** HF/d_6-DMSO digested UiO-67-Re and **b** UiO-67-Re soaked in d_4-CH_3OH

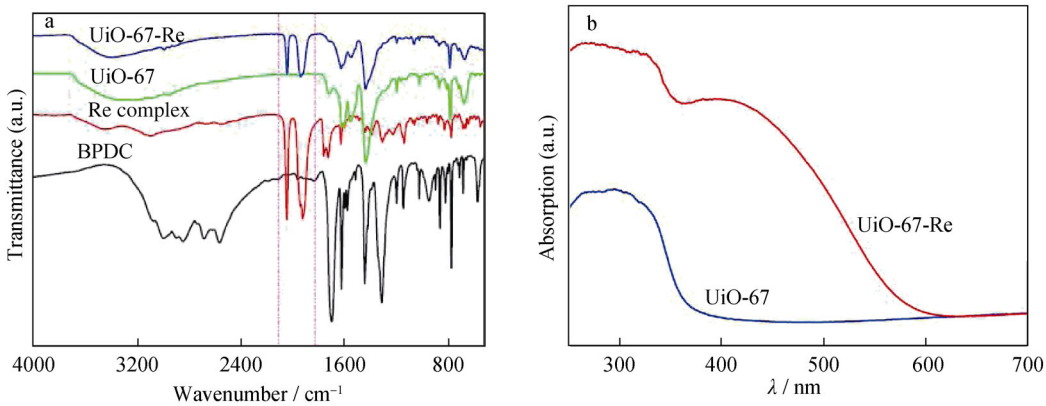

Fig. 5 **a** FTIR spectra of UiO-67-Re, UiO-67, Re complex and BPDC and **b** UV–Vis DRS of UiO-67-Re and UiO-67

the relative intensity of these characteristic bands is identical to that of the complex, indicating that the Re complex is intact in the MOF. UV–Vis spectroscopy of UiO-67-Re displays an extra absorption edge centered at 410 nm with an additional extended edge at 650 nm (Fig. 5b), consistent with the spectral features of the Re complex.

Considering the Re complex incorporated in the MOF, we expected that the UiO-67-Re can act as a catalyst in photocatalytic CO_2 reduction. Thus, UiO-67-Re was suspended in an aqueous solution containing 15% TEOA as the electron donor at pH = 8.5. As shown in Fig. 6a, UiO-67-Re is indeed a photocatalytic CO_2 reduction catalyst. Under the reaction conditions described above, CO product was detected. Comparing the activity of UiO-67-Re with that of Re complex at an equivalent concentration with Re metal center in UiO-67-Re, it shows that the photocatalytic activity of the MOF is preserved. Control experiments without Re complex detected no CO production. Additionally, we investigated the effect of the degree of PSLE on the activity of UiO-67-Re. The CO evolution rate of 100% Re complex incorporated into MOF is lower than that of 30% Re MOF, probably suggesting that the activity could depend on the extent of photon absorption by MOF [38]. However, more works needed to be carried out to further reveal the mechanism of the reduction reaction. Furthermore, in a photocatalytic system, the properties of solvent are also of importance. To this end, we investigated the influence of the solvent on the reaction activity of UiO-67-Re (Fig. 6b). As shown in Fig. 6b, the highest activity of UiO-67-Re was obtained using H_2O as solvent. On the contrary, the low activity was observed with CH_3CN, which is often employed as solvent in photocatalytic CO_2 reduction system. This result could be due to the decrease of the static dielectric constant of the mixture solution [38]. However, the stability of this system needs to be further improved. Further systematic studies are necessary to optimize the reaction condition and investigate the reaction mechanism.

4 Conclusion

PSLE process was developed as a mild and efficient method to build the functional MOF containing Re complex as CO_2 reduction catalyst. The resultant UiO-67-Re can be identified as a functional MOF that combines the advantages of molecular catalyst with an ordered and

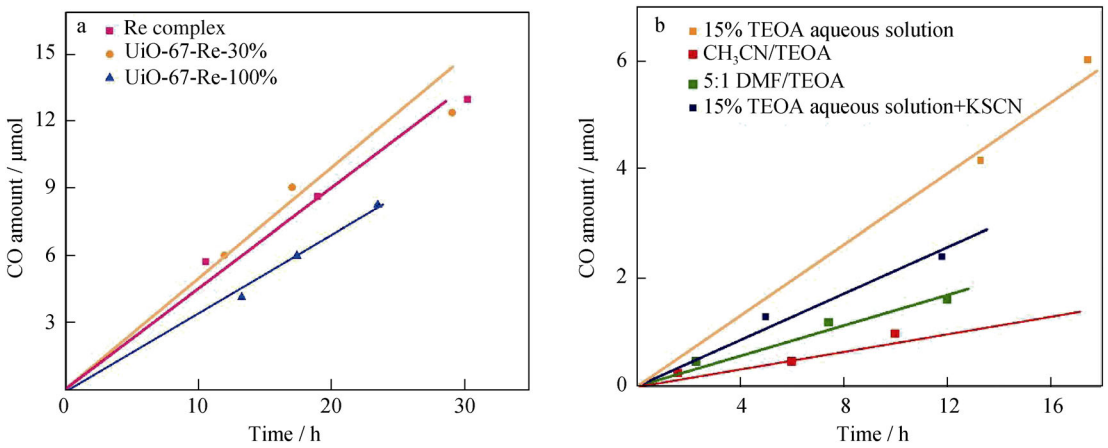

Fig. 6 Photocatalytic CO production in the presence of **a** UiO-67-Re-30%, UiO-67-Re-100% and Re complex, and **b** UiO-67-Re in different solvents. Conditions: 12 mg UiO-67-Re, 10 mg Re complex, 50 ml TEOA aqueous solution (15%); light source: 500 W Xe lamp with cut-off filter (> 420 nm)

stable MOF substrate. The structure of UiO-67-Re was confirmed by FTIR, NMR, XRD, and UV-vis. It exhibits efficient CO production. Incorporation of the Re complex in MOF can be expected to produce highly stable and easily recyclable material under the photocatalytic conditions.

Acknowledgements This work was financially supported by the National Natural Science Foundation of China (Nos.21773242 and 51772291).

References

[1] Liu C, Colón BC, Ziesack M, Silver PA, Nocera DG. Water splitting–biosynthetic system with CO_2 reduction efficiencies exceeding photosynthesis. Science. 2016;352(6290):1210.
[2] Gao H, Yue HH, Qi F, Yu B, Zhang WL, Chen YF. Few-layered ReS_2 nanosheets grown on graphene as electrocatalyst for hydrogen evolution reaction. Rare Met. 2018;37(12):1014.
[3] Wang S, Chen P, Bai Y, Yun JH, Liu G, Wang L. New $BiVO_4$ dual photoanodes with enriched oxygen vacancies for efficient solar-driven water splitting. Adv Mater. 2018;30(20):1800486.
[4] Zhao Y, Li Z, Li M, Liu J, Liu X, Waterhouse GIN, Wang Y, Zhao J, Gao W, Zhang Z, Long R, Zhang Q, Gu L, Liu X, Wen X, Ma D, Wu LZ, Tung CH, Zhang T. Reductive transformation of layered-double-hydroxide nanosheets to Fe-based heterostructures for efficient visible-light photocatalytic hydrogenation of CO. Adv Mater. 2018;30(36):1803127.
[5] Fan PD, Ji TH. Application research of MoS_2 nanosheets in catalysis and biology. Chin J Rare Met. 2018;42(4):429.
[6] Chen R, Wang P, Chen J, Wang C, Ao Y. Synergetic effect of MoS_2 and MXene on the enhanced H_2 evolution performance of CdS under visible light irradiation. Appl Surf Sci. 2019;473:11.
[7] Liu W, Shen J, Yang X, Liu Q, Tang H. Dual Z-scheme g-C_3N_4/Ag_3PO_4/Ag_2MoO_4 ternary composite photocatalyst for solar oxygen evolution from water splitting. Appl Surf Sci. 2018;456:369.
[8] Ao Y, Wang K, Wang P, Wang C, Hou J. Synthesis of novel 2D-2D p-n heterojunction BiOBr/$La_2Ti_2O_7$ composite photocatalyst with enhanced photocatalytic performance under both UV and visible light irradiation. Appl Catal B. 2016;194:157.
[9] Zhang L, Zhao ZJ, Gong J. Nanostructured materials for heterogeneous electrocatalytic CO_2 reduction and their related reaction mechanisms. Angew Chem Int Ed. 2017;56(38):11326.
[10] Huang H, Lin J, Zhu G, Weng Y, Wang X, Fu X, Long J. A long-lived mononuclear cyclopentadienyl ruthenium complex grafted onto anatase TiO_2 for Efficient CO_2 photoreduction. Angew Chem Int Ed. 2016;55(29):8314.
[11] Tu W, Zhou Y, Zou Z. Photocatalytic conversion of CO_2 into renewable hydrocarbon fuels: state-of-the-art accomplishment, challenges, and prospects. Adv Mater. 2014;26(27):4607.
[12] Cao S, Shen B, Tong T, Fu J, Yu J. 2D/2D heterojunction of ultrathin MXene/Bi_2WO_6 nanosheets for improved photocatalytic CO_2 reduction. Adv Funct Mater. 2018;28(21):1800136.
[13] Dong WH, Wu DD, Luo JM, Xing QJ, Liu H, Zou JP, Luo XB, Min XB, Liu HL, Luo SL, Au CT. Coupling of photodegradation of RhB with photoreduction of CO_2 over rGO/$SrTi_{0.95}Fe_{0.05}O_{3-\delta}$ catalyst: catalyst a strategy for one-pot conversion of organic pollutants to methanol and ethanol. J Catal. 2017;349:218.
[14] Zou JP, Chen Y, Liu SS, Xing QJ, Dong WH, Luo XB, Dai WL, Xiao X, Luo JM, Crittenden J. Electrochemical oxidation and advanced oxidation processes using a 3D hexagonal Co_3O_4 array anode for 4-nitrophenol decomposition coupled with simultaneous CO_2 conversion to liquid fuels via a flower-like CuO cathode. Water Res. 2019;150:330.
[15] Bai XF, Chen W, Wang BY, Feng GH, Wei W, Jiao Z, Sun YH. Recent progress on electrochemical reduction of carbon dioxide. Acta Phys Chim Sin. 2017;33(12):2388.
[16] Liu X, Inagaki S, Gong J. Heterogeneous molecular systems for photocatalytic CO_2 reduction with water oxidation. Angew Chem Int Ed. 2016;55(48):14924.
[17] Ou M, Tu W, Yin S, Xing W, Wu S, Wang H, Wan S, Zhong Q, Xu R. Amino-assisted anchoring of $CsPbBr_3$ perovskite quantum dots on porous g-C_3N_4 for enhanced photocatalytic CO_2 reduction. Angew Chem Int Ed. 2018;57(41):13570.
[18] Gao D, Cai F, Wang G, Bao X. Nanostructured heterogeneous catalysts for electrochemical reduction of CO_2. Curr Opin Green Sustain Chem. 2017;3:39.
[19] Xie H, Wang T, Liang J, Li Q, Sun S. Cu-based nanocatalysts for electrochemical reduction of CO_2. Nano Today. 2018;21:41.

[20] Takeda H, Koike K, Inoue H, Ishitani O. Development of an efficient photocatalytic system for CO_2 reduction using rhenium(I) complexes based on mechanistic studies. J Am Chem Soc. 2008;130(6):2023.
[21] Cohen SM. Postsynthetic methods for the functionalization of metal-organic frameworks. Chem Rev. 2011;112(2):970.
[22] Garcia H, Ferrer B. Photocatalysis by MOFs. In: i Xamena FX, Gascon J, editors. Metal Organic Frameworks as Heterogeneous Catalysts. Cambridge: Royal Society of Chemistry; 2103. 365.
[23] Tian L, Yang X, Liu Q, Qu F, Tang H. Anchoring metal-organic framework nanoparticles on graphitic carbon nitrides for solar-driven photocatalytic hydrogen evolution. Appl Surf Sci. 2018;455:403.
[24] Liu MR, Hong QL, Li QH, Du Y, Zhang HX, Chen S, Zhou T, Zhang J. Cobalt boron imidazolate framework derived cobalt nanoparticles encapsulated in B/N codoped nanocarbon as efficient bifunctional electrocatalysts for overall water splitting. Adv Funct Mater. 2018;28(26):1801136.
[25] Xiao JD, Han L, Luo J, Yu SH, Jiang HL. Integration of plasmonic effects and Schottky junctions into metal-organic framework composites: steering charge flow for Enhanced visible-light photocatalysis. Angew Chem Int Ed. 2018;57(4):1103.
[26] Meyer K, Ranocchiari M, van Bokhoven JA. Metal organic frameworks for photo-catalytic water splitting. Energy Environ Sci. 2015;8(7):1923.
[27] Wang S, Yao W, Lin J, Ding Z, Wang X. Cobalt imidazolate metal-organic frameworks photosplit CO_2 under mild reaction conditions. Angew Chem Int Ed. 2014;53(4):1034.
[28] Zhang T, Lin W. Metal-organic frameworks for artificial photosynthesis and photocatalysis. Chem Soc Rev. 2014;43(16):5982.
[29] Zhu QL, Xu Q. Metal-organic framework composites. Chem Soc Rev. 2014;43(16):5468.
[30] Gomes Silva C, Luz I, Llabrés i Xamena FX, Corma A, García H. Water stable Zr–benzenedicarboxylate metal–organic frameworks as photocatalysts for hydrogen generation. Chem Eur J. 2010;16(36):11133.
[31] Fateeva A, Chater PA, Ireland CP, Tahir AA, Khimyak YZ, Wiper PV, Darwent JR, Rosseinsky MJ. A water-stable porphyrin-based metal-organic framework active for visible-light photocatalysis. Angew Chem Int Ed. 2012;51(30):7440.
[32] Long J, Wang S, Ding Z, Wang S, Zhou Y, Huang L, Wang X. Amine-functionalized zirconium metal-organic framework as efficient visible-light photocatalyst for aerobic organic transformations. Chem Commun. 2012;48(95):11656.
[33] Xu HQ, Hu J, Wang D, Li Z, Zhang Q, Luo Y, Yu SH, Jiang HL. Visible-light photoreduction of CO_2 in a metal-organic framework: boosting electron-hole separation via electron trap states. J Am Chem Soc. 2015;137(42):13440.
[34] Chen EX, Qiu M, Zhang YF, Zhu YS, Liu LY, Sun YY, Bu X, Zhang J, Lin Q. Acid and base resistant zirconium polyphenolate-metalloporphyrin scaffolds for efficient CO_2 photoreduction. Adv Mater. 2018;30(2):1704388.
[35] Wang D, Huang R, Liu W, Sun D, Li Z. Fe-based MOFs for photocatalytic CO_2 reduction: role of coordination unsaturated sites and dual excitation pathways. ACS Catal. 2014;4(12):4254.
[36] Wang C, Xie Z, deKrafft KE, Lin W. Doping metal-organic frameworks for water oxidation, carbon dioxide reduction, and organic photocatalysis. J Am Chem Soc. 2011;133(34):13445.
[37] Wang C, Wang JL, Lin W. Elucidating molecular iridium water oxidation catalysts using metal-organic frameworks: a comprehensive structural, catalytic, spectroscopic, and kinetic study. J Am Chem Soc. 2012;134(48):19895.
[38] Zhou T, Du Y, Borgna A, Hong J, Wang Y, Han J, Zhang W, Xu R. Post-synthesis modification of a metal-organic framework to construct a bifunctional photocatalyst for hydrogen production. Energy Environ Sci. 2013;6(11):3229.
[39] Xiao JD, Jiang HL. Metal-organic frameworks for photocatalysis and photothermal catalysis. Acc Chem Res. 2018;51(4):910.
[40] Li R, Hu J, Deng M, Wang H, Wang X, Hu Y, Jiang HL, Jiang J, Zhang Q, Xie Y, Xiong Y. Integration of an inorganic semiconductor with a metal-organic framework: a platform for enhanced gaseous photocatalytic reactions. Adv Mater. 2014;26(28):4783.
[41] Sun D, Fu Y, Liu W, Ye L, Wang D, Yang L, Fu X, Li Z. Studies on photocatalytic CO_2 reduction over NH_2-Uio-66(Zr) and its derivatives: towards a better understanding of photocatalysis on metal-organic frameworks. Chem Eur J. 2013;19(42):14279.
[42] Lei Z, Xue Y, Chen W, Qiu W, Zhang Y, Horike S, Tang L. MOFs-based heterogeneous catalysts: new opportunities for energy-related CO_2 conversion. Adv Energy Mater. 2018;8(32):1801587.
[43] Li F, Wang D, Xing QJ, Zhou G, Liu SS, Li Y, Zheng LL, Ye P, Zou JP. Design and syntheses of MOF/COF hybrid materials via postsynthetic covalent modification: an efficient strategy to boost the visible-light-driven photocatalytic performance. Appl Catal B. 2019;243:621.
[44] Fu Y, Sun D, Chen Y, Huang R, Ding Z, Fu X, Li Z. An amine-functionalized titanium metal-organic framework photocatalyst with visible-light-induced activity for CO_2 reduction. Angew Chem Int Ed. 2012;51(14):3364.
[45] Pullen S, Fei H, Orthaber A, Cohen SM, Ott S. Enhanced photochemical hydrogen production by a molecular diiron catalyst incorporated into a metal-organic framework. J Am Chem Soc. 2013;135(45):16997.
[46] Kim M, Cahill JF, Su Y, Prather KA, Cohen SM. Postsynthetic ligand exchange as a route to functionalization of 'inert' metal-organic frameworks. Chem Sci. 2012;3(1):126.
[47] Schaate A, Roy P, Godt A, Lippke J, Waltz F, Wiebcke M, Behrens P. Modulated synthesis of Zr-based metal-organic frameworks: from nano to single crystals. Chem Eur J. 2011;17(24):6643.
[48] Kim M, Cahill JF, Fei H, Prather KA, Cohen SM. Postsynthetic ligand and cation exchange in robust metal-organic frameworks. J Am Chem Soc. 2012;134(43):18082.